Efficient Double- And Triple-Junction Nonfullerene Organic Photovoltaics and Design Guidelines for Optimal Cell Performance

Firdaus, Yuliar; Ho, Carr Hoi Yi; Lin, Yuanbao; Yengel, Emre; Le Corre, Vincent M.; Nugraha, Mohamad I.; Yarali, Emre; So, Franky; Anthopoulos, Thomas D.

Published in:
ACS Energy Letters

DOI:
10.1021/acsenergylett.0c02077

Publication date:
2020

ACS Energy LETTERS

http://pubs.acs.org/journal/aelccp

LETTER

Efficient Double- and Triple-Junction Nonfullerene Organic Photovoltaics and Design Guidelines for Optimal Cell Performance

Yuliar Firdaus,* Carr Hoi Yi Ho, Yuanbao Lin, Emre Yengel, Vincent M. Le Corre, Mohamad I. Nugraha, Emre Yarali, Franky So, and Thomas D. Anthopoulos*

Cite This: *ACS Energy Lett.* 2020, 5, 3692–3701

Read Online

ACCESS | Metrics & More | Article Recommendations | Supporting Information

ABSTRACT: The performance of multijunction devices lags behind single-junction organic photovoltaics (OPVs) mainly because of the lack of suitable subcells. Here, we attempt to address this bottleneck and demonstrate efficient nonfullerene-based multijunction OPVs while at the same time highlighting the remaining challenges. We first demonstrate double-junction OPVs with power conversion efficiency (PCE) of 16.5%. Going a step further, we developed triple-junction OPVs with a PCE of 14.9%, the highest value reported to date for this triple-junction cells. Device simulations suggest that improving the front-cell's carrier mobility to >5 × 10^{-4} cm^2 V^{-1} s^{-1} is needed to boost the efficiency of double- and triple-junction OPVs. Analysis of the efficiency limit of triple-junction devices predicts that PCE values of close to 26% are possible. To achieve this, however, the optical absorption and charge transport within the subcells would need to be optimized. The work is an important step toward next-generation multijunction OPVs.

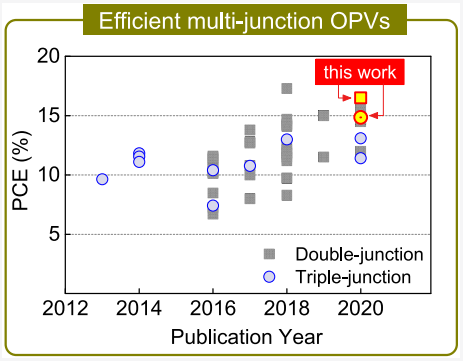

The advent of new nonfullerene acceptor (NFA) molecules has led to a rapid increase in the power conversion efficiency (PCE) of organic photovoltaics (OPVs).[1−4] To increase the efficiency of OPVs further, the absorption range of the photoactive materials is essential, which in general can be achieved via two main approaches. The first is to construct a binary or ternary single-junction (SJ) device, where the active layer is composed of donor and acceptor materials with complementary absorption.[2−7] Very recently, a new electron-deficient-core-based fused ring NFA, namely Y6,[3] with the features of a high electron mobility, long-range exciton diffusion length,[8] and broad absorption range up to 930 nm was reported. When paired with polymer donor PM6 (absorb up to 700 nm), the PM6:Y6-based OPVs achieved a breakthrough in PCE of 15.7%.[3] Since then, the PCE of SJ OPVs has reached over 18% using Y6 and its derivatives as the acceptor.[4−7,9,10]

An alternative approach is to construct a multijunction OPV or hybrid where two or more subcells with complementary absorption spectra are connected in series.[11−16] Unfortunately, most of the reported tandem [double-junction (DJ)] OPVs currently exhibit PCEs below 15% (Table S1), with only a handful of values reaching >16%.[13,17] The same is true for triple-junction (TJ) OPVs where only a few studies reported cells with PCE > 13% (Table S3).[18,19] One common technical challenge often associated with multijunction OPVs' performance limitations is the lack of efficient, wide-bandgap (optical bandgap, E_g > 1.7 eV) active-layers for the front cell.[11,12,17,20] This is because the field of NFA-based SJ OPVs has focused almost exclusively on the development of low bandgap materials (<1.5 eV),[2,3,21,22] while wide-bandgap NFAs have received significantly less attention.[12,20] However, it is not apparent which aspects of the wide-bandgap NFA still need to be improved. Moreover, the use of subcells with minimal absorption overlap is critical to achieving high-efficiency multijunction OPVs, which again has proven challenging to realize experimentally.[23] Thus, in order to improve the

Received: September 27, 2020
Accepted: October 26, 2020
Published: November 12, 2020

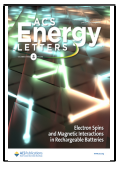

https://dx.doi.org/10.1021/acsenergylett.0c02077
ACS Energy Lett. 2020, 5, 3692–3701

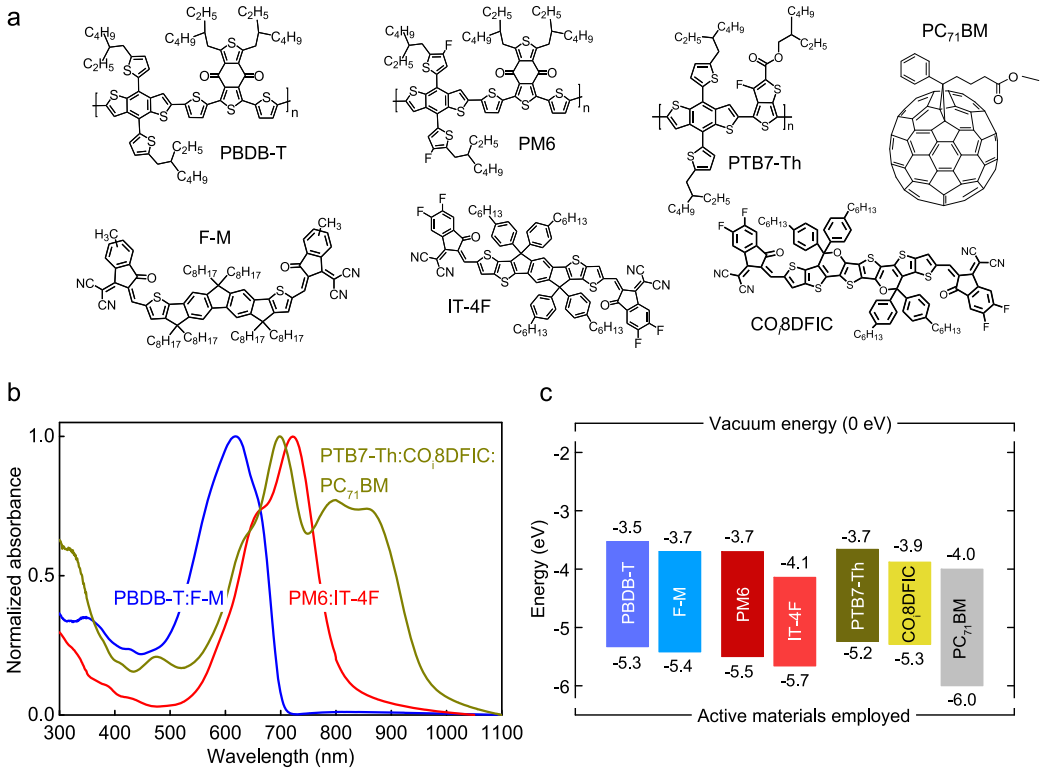

Figure 1. (a) Chemical structure of active-layer (donor and acceptor) materials used. (b) Normalized absorbance of the photoactive blends used for the front-cell (FC) (PBDB-T:F-M) and the back-cell (BC) (PTB7-Th:CO$_i$8DFIC:PC$_{71}$BM) of the double-junction (DJ) OPVs. The absorbance of the middle-cell (MC) (PM6:IT-4F) used in the TJ device (Figure 4) is also shown. (c) Energy levels of the donor and acceptor materials used in this work.[2,3,17,20]

performance of multijunction OPVs further, the factors limiting their performance need to be identified and addressed.

Here, we describe the development of efficient DJ and TJ OPVs while simultaneously drawing important cell-design rules to aid the development of higher-efficiency multijunction OPVs. First, we show that a DJ device with a high PCE of 16.5% can be obtained when PBDB-T:F-M and PTB7-Th:CO$_i$8DFIC:PC$_{71}$BM (full chemical names are given in the Supporting Information) are used as the front-cell (FC) and the back-cell (BC), respectively. For the interconnecting layer (ICL) we employ the recently reported PEDOT:PSS HTL Solar (HSolar) as the hole transport layer (HTL) and ZnO nanoparticle (NP) as the electron transport layer (ETL).[13] Second, we demonstrate TJ OPVs with PCE of 14.9%, one of the highest values reported to date. We achieved this using FC, middle-cell (MC), and BC with optical bandgaps of 1.75, 1.53, and 1.3 eV, respectively. Our modeling analyses show that one of the critical parameters for high performing DJs is the low bimolecular recombination in PBDB-T:F-M FC. We also find that the carrier mobility in PBDB-T:F-M FC ($<10^{-4}$ cm^2 V^{-1} s^{-1}) limits the device performance and would need to be increased in order to achieve PCEs of >18%. Moreover, reducing the bimolecular recombination rate and the energy-loss in the back cell could boost the PCE to >19%. Our calculations also suggest that complementary absorption between the three subcells in the TJ device could be further optimized when bandgaps of 2, 1.57, and 1.2 eV for the FC, MC, and BC, respectively, are employed. This combined with an increase in the carrier mobilities to $>10^{-3}$ cm^2 V^{-1} s^{-1} for all subcells is predicted to yield maximum PCE of >26%.

Figure 1a shows the chemical structures of the donor polymers and acceptors used as active materials in this work, while Figure 1b displays the absorbance of the donor and acceptor blend films. The PBDB-T:F-M blend absorbs strongly in the visible range between 450 and 710 nm, and the PM6:IT-4F blend absorbs in the range of 550−820 nm; the PTB7-Th:CO$_i$8DFIC:PC$_{71}$BM blend absorbs in the spectral range of 550−1000 nm. Figure 1c depicts the corresponding energy levels of the materials used.

To fabricate DJ cells, PBDB-T:F-M BHJ[20] was used as the FC and combined with the near-infrared (NIR) absorbing PTB7-Th:CO$_i$8DFIC:PC$_{71}$BM[24] BHJ as the BC. The two subcells were integrated to form two-terminal inverted DJ OPVs (Figure 2a) using solution processing,[13] except for the top MoO_3/Ag electrode which was thermally evaporated. Further details on the cell fabrication can be found in the Supporting Information. The schematic energy diagram of each layer in the DJ is shown in Figure 2b, indicating the proper energy level alignment of each component in the device. The optimization of DJ OPVs was supported by optical and electrical simulation, the combination of which enabled us to predict the optimal active layer thicknesses of each subcell.[12,25] The MATLAB program combines optical transfer matrix modeling and the analysis of the measured current density−voltage (J−V) curves for the SJ devices used as the subcells. First, the J−V curve of each SJ device of different thicknesses is measured, and the current values for each J−V curve are normalized to the respective J_{SC}. Next, we use transfer matrix modeling and calculate the SJ quantum efficiency (QE) term to predict the J_{SC} of each subcell when incorporated in the DJ device. The predicted J_{SC} values for

https://dx.doi.org/10.1021/acsenergylett.0c02077
ACS Energy Lett. 2020, 5, 3692−3701

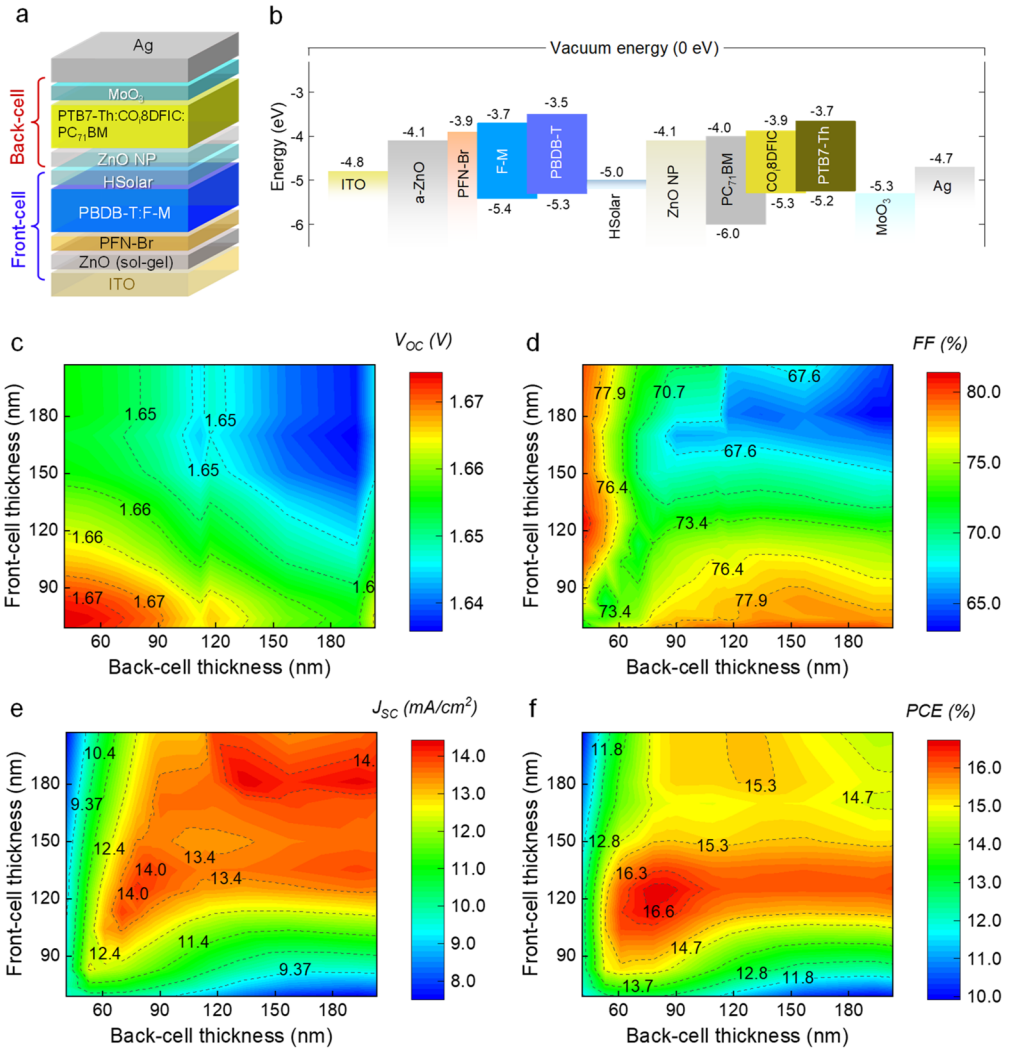

Figure 2. (a) DJ solar cell device structure. (b) Energy diagram of each layer of the DJ device. Figures of merit of DJ solar cell devices predicted from optical−electrical modeling: (c) V_{OC}, (d) FF, (e) J_{SC}, and (f) PCE.

each subcell were then multiplied by their respective normalized SJ $J-V$ curves to predict the complete $J-V$ characteristic of each subcell in the DJ OPV. Last, we apply Kirchhoff's laws to construct the overall $J-V$ curve for the DJ OPV device.[26] Figure S1 provides the optical constant of the layers in the DJ cell and the measured $J-V$ curves of PBDB-T:F-M and PTB7-Th:CO_i8DFIC:$PC_{71}BM$-based SJ cells with different thicknesses. Figure 2c−f describes the modeling analyses, emphasizing the specific subcell thickness combinations amenable to the best DJ figure of merits. The model predicts that V_{OC} and FF would decrease, whereas J_{SC} would increase to >14 mAcm^{-2} when the subcells' thicknesses increase (Figure 2c−e). PCE values in excess of 16% are predicted for various subcell thickness combinations, and particularly when an FC with thickness between 100 and 140 nm and a BC with a thickness in the range of 60−110 nm are utilized (Figure 2f). The model also predicts that DJ OPVs utilizing FCs and BCs with thicknesses of 125 and 85 nm, respectively, should yield the highest PCE of 16.7%.

DJ solar cells based on PBDB-T:F-M as the FC and PTB7-Th:CO_i8DFIC:$PC_{71}BM$ as the BC were constructed with optimal subcell thickness combinations chosen in the ranges established from the optical and electrical modeling analyses. Using a thickness combination of 130 nm for the FC and 100 nm for the BC, a DJ OPV with a maximum PCE of 16.5% (Figure 3a and Table 1) was obtained, a result consistent with the predicted PCE for this specific combination of subcell thicknesses. The experimental $J-V$ curves for the constructed DJ OPVs and those predicted by the model are superimposed in Figure 3a, while the figures of merit of the corresponding DJ device are summarized in Table 1 for comparison. Optimized DJ cells exhibit an FF of 71.8%, V_{OC} of 1.66 V, and a maximum J_{SC} of 13.9 mA cm^{-2}.

The box charts in Figure 3b present the statistical distribution of the various figure of merits of the DJ cells calculated from 30 devices. Evidently, the DJ OPVs show a small V_{OC} variation of less than 0.01 V. On the other hand, the J_{SC} varies between 13.6 and 14.3 mA cm^{-2}, while FF shows a small variation of 1.28% between devices, which is believed to originate mainly from unintentional changes in active layer thickness in agreement with our simulations. The ensuing DJ OPVs yield PCE values of >16%, in agreement with the modeling predictions (Figure 2f). Overall, all devices show excellent performance with small PCE variation (average PCE = 16.3%). The efficiency enhancement factor of the DJ devices, defined as the percentage increase of PCE of the DJ cell from the more efficient SJ cell utilized, is nearly 30% (Table 1) and demonstrates the success of the approach.

https://dx.doi.org/10.1021/acsenergylett.0c02077
ACS Energy Lett. 2020, 5, 3692−3701

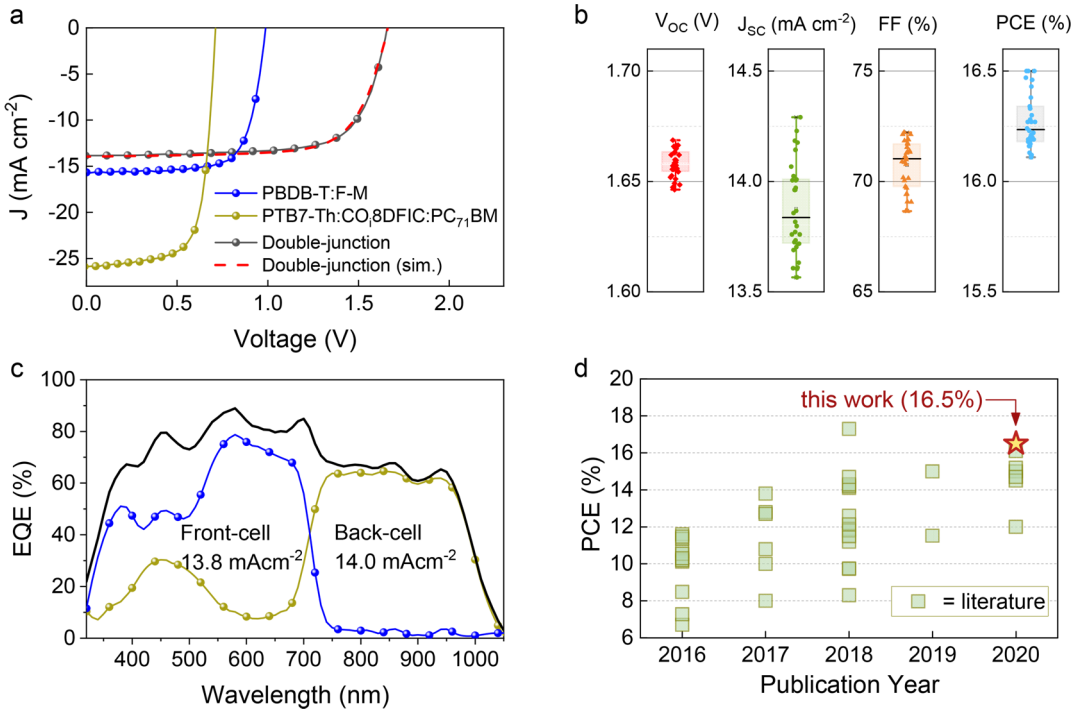

Figure 3. (a) *J*−*V* curves of the DJ cells and PBDB-T:F-M, and PTB7-Th:CO$_i$8DFIC:PC$_{71}$BM SJ cells with their thicknesses optimized for the DJ cells. *J*−*V* curves of the DJ cells superimposed with that predicted from optical and electrical modeling (125 nm FC and a 85 nm BC). (b) Box charts of measured V_{OC}, J_{SC}, FF, and PCE of the DJ device (total number of devices is 30). (c) EQE of the optimized DJ solar cells. (d) Comparison of organic DJ PCEs reported from 2016 onward.[12,13,17,18,20,24,27−55] Details about the DJ cells from the literature are given in Table S1.

Table 1. Photovoltaic Parameters of Optimized SJs (with Respective Active-Layer Used As Subcells in DJ OPV) and DJ OPVs Obtained Experimentally (Exp) and from Simulations (Sim)[a]

cell type/BHJ	thickness (nm)	condition	V_{OC} (V)	J_{SC} (mA cm^{-2})	FF (%)	PCE (%)
PBDB-T:F-M SJ	130	average	0.98 ± 0.004	15.4 ± 0.26	71.7 ± 0.95	10.9 ± 0.26
		maximum	0.99	15.7	73.1	11.3
PTB7-Th: CO$_i$8DFIC:PC$_{71}$BM SJ	110	average	0.71 ± 0.003	25.5 ± 0.37	70.4 ± 0.68	12.7 ± 0.17
		maximum	0.71	25.9	71.0	13.1
DJ device (Exp)	130/100	average	1.66 ± 0.01	13.9 ± 0.26	70.5 ± 1.28	16.3 ± 0.11
		maximum	1.66	13.9	71.8	16.5
DJ device (Sim)	125/85		1.66	13.9	72.5	16.7

[a]The deviation for each parameter was calculated from 30 devices.

To better understand the origin of the improved cell performance, we performed EQE measurements. Optimized DJ devices (Figure 3c) show an average EQE of 67% in the absorption range from 300 to 1000 nm. The FC's EQE was also evaluated by exciting it with 850 nm light bias using an inorganic light-emitting diode (LED). The obtained EQE spectra show a strong response between 300 to 730 nm with a maximum EQE of 77% at around 570 nm. The BC's EQE (obtained by applying 595 nm light bias) absorbs mainly low energy photons in the range 700−1050 nm with a maximum EQE of ≈64%. The FC gave an integrated J_{SC} of 13.8 mAcm^{-2} closely matching the integrated J_{SC} of the BC (14 mAcm^{-2}) and similar to the tandem cell's J_{SC} of 13.9 mAcm^{-2} measured under simulated solar illumination (Table 1).

To compare our results with those found in the literature, we plotted all high PCE values reported for DJ OPVs from 2016 onward (Figure 3d).[12,13,17,18,20,24,27−55] Evidently, the maximum PCE of DJ OPVs developed here is among the highest values reported to date (details of the DJ cells found in the literature are provided in Table S1). In particular, DJ OPVs with PCE of over 16% have been reported only twice before, one study by Meng et al. (PCE = 17.3%)[17] and our own recent study by Ho et al., (PCE of 16.1%),[13] with all three studies (including this work) relying on the use of PBDB-T:F-M for the FC. Previously, we showed that the PCE for DJ OPVs is maximized when the FC and BC's optical bandgap is in the range of 1.6−2.0 eV and 1.2−1.5 eV, respectively.[11] Therefore, PBDB-T:F-M cells offer attractive absorption spectrum as an FC (1.75 eV) yielding high J_{SC} and FF. The PTB7-Th:CO$_i$8DFIC:PC$_{71}$BM- BC on the other hand has an E_g of ∼1.3 eV and as such provides the required complementary absorption to PBDB-T:F-M, along with high J_{SC} and FF (Table 1).

Next, we examined the potential of TJ architecture as it offers additional opportunities to improve the V_{OC}, which is important for various energy-related applications such as water splitting.[25,62] We fabricated TJ OPVs by employing PM6:IT-4F[63] as the MC and with the same FC and BC as those used in

https://dx.doi.org/10.1021/acsenergylett.0c02077
ACS Energy Lett. 2020, 5, 3692−3701

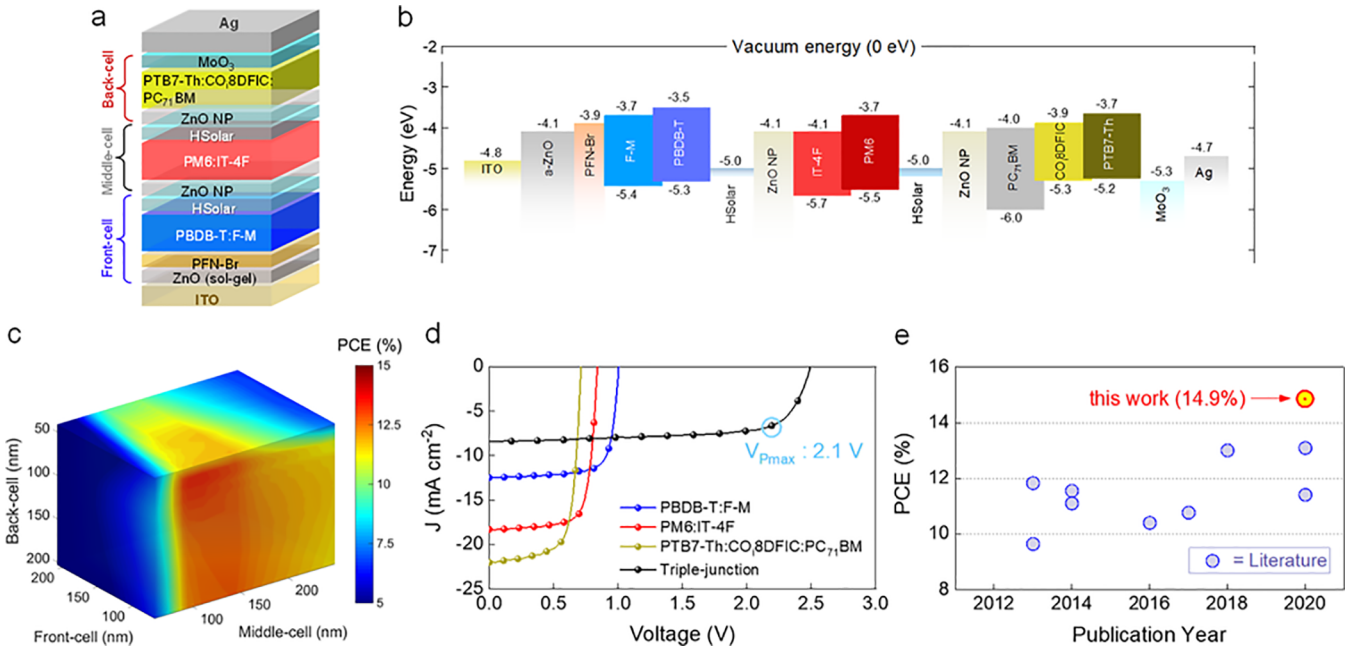

Figure 4. (a) Triple-junction (TJ) solar cell device structure. (b) Energy diagram of each layer of the TJ device. (c) PCE of TJ cells predicted from combined optical and electrical modeling for subcells combination shown in Figure 4a. (d) *J*−*V* curves of measured TJ cell with an optimized thickness combination (75 nm front cell, a 110 nm MC, and a 60 nm back cell). *J*−*V* curves of the PBDB-T:F-M, PM6:IT-4F, PTB7-Th:CO_i8DFIC:PC_{71}BM SJ are also shown (their respective thicknesses optimized for the TJ cells). (e) Comparison of organic TJ PCEs reported from 2013 onward.[18,19,25,56−61] Details about the TJ cells from the literature can be found in Table S3.

Table 2. Photovoltaic Parameters of Optimized SJs (with Respective Active-Layer Used as Subcells in TJ OPV) and TJ OPVs[a]

cell type/BHJ	thickness (nm)	condition	V_{OC} (V)	J_{SC} (mA cm^{-2})	FF (%)	PCE (%)
PBDB-T:F-M SJ	75	average	1.00 ± 0.002	12.5 ± 0.07	74.5 ± 1.33	9.4 ± 0.22
		maximum	1.00	12.5	75.6	9.5
PM6:IT-4F SJ	110	average	0.83 ± 0.008	18.8 ± 0.51	74.5 ± 0.63	11.7 ± 0.25
		maximum	0.83	19.1	75.4	11.95
PTB7-Th: CO_i8DFIC:PC_{71}BM SJ	65	average	0.71 ± 0.005	22.5 ± 0.81	69.3 ± 2.06	11.1 ± 0.29
		maximum	0.71	23.2	71.0	11.7
TJ device (Exp)	75/110/65	average	2.49 ± 0.015	8.1 ± 0.24	70.5 ± 1.21	14.2 ± 0.34
		maximum	2.49	8.4	70.8	14.9
TJ device (Sim)	80/110/60		2.54	8.2	71.3	14.9

[a]From experiment (Exp) and simulation (Sim). Device statistics from 15 devices.

the DJ OPVs previously. We chose the PM6:IT-4F BHJ (E_g: 1.53 eV) as it provides complementary absorption with the two other subcells (Figure 1b). Figure 4a illustrates the TJ device configuration using the same HSolar/ZnO NP ICL between the three subcells. The schematic energy diagram of each layer in the TJ is shown in Figure 4b. Following the same approach as depicted for the DJ solar cells, we first examined the expected performance of the TJ devices using combined optical and electrical modeling (Figure 4c). Figure S2a,b provides the optical constant of the PM6:IT-4F and the measured *J*−*V* curves of PM6:IT-4F-based SJ cells with different thicknesses. The model predicts PCEs as high as 14.9% for a TJ device composed of an 80 nm FC, a 110 nm MC, and a 60 nm BC. The EQEs of the PBDB-T:F-M, PM6:IT-4F, and PTB7-Th:CO_i8DFIC:PC_{71}BM-based SJ devices at those respective thicknesses are shown in Figure S2c. We then constructed the corresponding TJ device, demonstrating a champion device with FF = 70.8%, J_{SC} = 8.4 mAcm^{-2}, V_{OC} = 2.49 V, and a superb PCE of 14.9% (Figure 4d), in good agreement with our simulation (Table 2). The PCE is the highest achieved to date with a TJ OPV (Figure 4e).[18,19,25,56−61] As depicted in Figure 4d, the TJ solar cells also yield remarkably high operating voltages (V_{Pmax}) of 2.1 V; defined as the voltage at the maximum power point ($J_{Pmax} \approx 7$ mA cm^{-2}).

To examine the key factors that limit the performance of the DJ OPV, we performed drift-diffusion simulations (Setfos 4.6, FLUXIM AG)[11,12,64,65] for the PBDB-T:F-M and ternary PTB7-Th:CO_i8DFIC:PC_{71}BM SJ cells. The simulation describes charge transport and recombination with the latter following a reduced Langevin recombination given by[12,66]

$$k_{BMR} = \gamma_{pre} k_L = \gamma_{pre} \frac{q}{\varepsilon_r \varepsilon_0} (\mu_h + \mu_e) \quad (1)$$

Here, γ_{pre} is the recombination prefactor, k_L is the Langevin recombination, $\varepsilon_r\varepsilon_0$ is the material dielectric constant, and μ_h/μ_e are the hole/electron mobilities. Details about the simulation can be found in the Supporting Information.

We simulated PBDB-T:F-M, PBDB-T:IDTTA, and the ternary PTB7-Th:CO_i8DFIC:PC_{71}BM SJ cells of different thicknesses using a value of k_{BMR} (eq 1) and the appropriate space charge limited current (SCLC) charge-carrier mobilities

https://dx.doi.org/10.1021/acsenergylett.0c02077
ACS Energy Lett. 2020, 5, 3692−3701

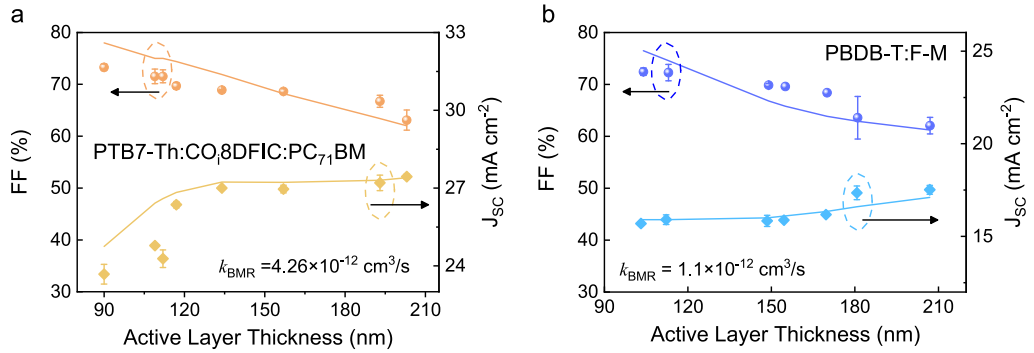

Figure 5. Experimentally measured (symbol) and simulated (solid line) fill-factor (FF) and short-circuit current density (J_{SC}) versus active-layer thickness for (a) PTB7-Th:CO$_i$8DFIC:PC$_{71}$BM and (b) PBDB-T:F-M BHJ solar cells. The legends in both figures show the corresponding bimolecular recombination rate employed in the simulation. The input parameters used for the simulation can be found in Table S2.

Table 3. Summary of Results of DJ and TJ OPV Simulations

DJ Design Rule[a]								
case	E_{CT} (eV)	$k_{BMR,FC}$ (cm^3 s^{-1})	$k_{BMR,BC}$	μ_{FC} ($\mu_h = \mu_e$) (cm^2 V^{-1} s^{-1})	V_{OC} (V)	J_{SC} (mAcm^{-2})	FF (%)	PCE (%)
1. FC/BC1	1.57/1.30	10^{-12}	4×10^{-12}	2×10^{-4}	1.67	13.1	77	16.9
				5×10^{-4}	1.67	13.5	80	18.1
				1×10^{-3}	1.67	13.5	82	18.5
				2×10^{-3}	1.67	13.5	83	18.8
				5×10^{-3}	1.66	13.5	84	18.9
2. FC/BC1	1.57/1.30	10^{-12}	10^{-12}	2×10^{-4}	1.70	13.5	77	17.6
				5×10^{-4}	1.70	13.6	82	18.9
				1×10^{-3}	1.70	13.6	84	19.4
				2×10^{-3}	1.70	13.6	85	19.7
				5×10^{-3}	1.70	13.6	86	19.8
3. FC/BC2	1.57/1.40	10^{-12}	10^{-12}	2×10^{-4}	1.70	13.8	77	18.9
				5×10^{-4}	1.70	13.8	82	20.3
				1×10^{-3}	1.70	13.8	84	20.9
				2×10^{-3}	1.70	13.8	85	21.2
				5×10^{-3}	1.70	13.8	86	21.4
TJ Design Rule[b]								
case	E_{CT} [FC/MC/BC] (eV)	$\mu_h = \mu_e$ (cm^2 V^{-1} s^{-1})	IQE (%)	$th_{FC}/th_{MC}/th_{BC}$[c] (nm)	V_{OC} (V)	J_{SC} (mAcm^{-2})	FF (%)	PCE (%)
1	1.95/1.52/1.25	5×10^{-4}	90	100/80/65	3.03	9.0	88	23.9
2	1.95/1.52/1.15	5×10^{-4}	90	130/110/65	2.90	9.6	87	24.1
3	1.95/1.41/1.25	5×10^{-4}	90	100/80/65	2.92	8.4	89	21.8
4	1.95/1.41/1.15	5×10^{-4}	90	190/80/95	2.79	10.0	84	23.4
5	1.65/1.52/1.25	5×10^{-4}	90	100/110/65	2.73	8.1	87	19.4
6	1.65/1.52/1.15	5×10^{-4}	90	100/110/65	2.61	8.3	88	19.2
7	1.65/1.41/1.25	5×10^{-4}	90	100/80/65	2.63	7.9	87	18.0
8	1.65/1.41/1.15	5×10^{-4}	90	100/110/95	2.50	9.1	86	19.7
9	1.95/1.52/1.25	10^{-3}	95	100/80/65	3.04	9.5	89	25.7
10	1.95/1.52/1.15	10^{-3}	95	130/110/95	2.90	10.2	88	26.0

[a]Additional DJ simulation parameters: charge mobility for all back-cell in DJ simulation: $\mu_h = 6 \times 10^{-4}$ cm^2 V^{-1} s^{-1}, $\mu_e = 5 \times 10^{-4}$ cm^2 V^{-1} s^{-1}; IQE for all subcells = 90%; E_{CT}, charge-transfer state energy. [b]Additional TJ device simulation: $E_{CT} = E_g - 0.05$ eV; $k_{BMR} = 10^{-12}$ cm^3 s^{-1}; charge mobilities of FC, MC, and BC are the same. [c]th: thicknesses of the subcells.

from Table S2. Only one fit parameter, γ_{pre}, was used to simulate a wide variety of experimental devices with FF varying from 60% to 75%. We obtained an excellent agreement between the experimental and simulated FF and J_{SC} for the ternary PTB7-Th:CO$_i$8DFIC:PC$_{71}$BM device for different BHJ thicknesses when a recombination prefactor ($\gamma_{pre} = k_{BMR}/k_L$) of 0.007 and a k_L value of 6.1×10^{-10} cm^3 s^{-1} were used as fitting parameters (Table S2).

The relatively high charge mobility (Table S2) and low γ_{pre} explain why the FFs of the ternary devices are high (>65%) for a wide range of active layer thicknesses up to 200 nm (Figure 5a). Similar analyses performed on PBDB-T:F-M cells show that the FFs are >65% when the active layer thicknesses are <180 nm (Figure 5b). We attribute this to the low γ_{pre} value of the cell (0.005), although the electron mobility is low too (<10^{-4} cm^2 V^{-1} s^{-1}). For comparison, another wide bandgap PBDB-T:IDTTA blend reported recently exhibits comparable charge transport but higher γ_{pre} (0.016) that leads to lower FF (Figure S3a).[12] The γ_{pre} value of the PBDB-T:IDTTA device obtained from the modeling analyses is in excellent agreement

https://dx.doi.org/10.1021/acsenergylett.0c02077
ACS Energy Lett. 2020, 5, 3692−3701

with the γ_{pre} value inferred from the transport and recombination analyses.[12,66] Because of its lower FF, the DJ utilizing PBDB-T:IDTTA as the FC yields a maximum PCE of 15%.

Given the above analysis, the high FF and PCE of DJ OPV can be achieved because of the low γ_{pre} of devices. However, we also notice that the electron mobility of PBDB-T:F-M BHJ is only $\sim 10^{-4}$ cm^2 V^{-1} s^{-1}, which limits the PCE of the DJ cells. To verify this hypothesis we calculated the PCE of the DJ following our previous approach,[11] which is similar to the analysis described for Figure 2c–f. In brief, the J–V curve of each individual subcell was simulated using the numerical simulator Setfos 4.4 and subsequently combined with transfer matrix modeling (MATLAB) to construct the J–V curve of the DJ device. Figure S3b shows the extinction coefficients of the FC and BC used in the simulation and inferred from ellipsometry measurements. The FC's absorption is based on PBDB-T:F-M blend absorption, whereas the BC absorption is based on different blends (**BC1**, ternary PTB7-Th:CO$_i$8DFIC:PC$_{71}$BM; **BC2**, PM6:Y6). The specific BC absorption profiles were chosen because they provide complementary absorption to the PBDB-T:F-M-based FC. For a DJ cell with absorption profiles of FC/BC1 (case 1), and assuming different $\mu_{h,e}$ and k_{BMR} (Table 3), the PCE is predicted to increase to 18.1% and 18.9% if the FC carrier mobility increases to 5×10^{-4} and 5×10^{-3} cm^2 V^{-1} s^{-1}, respectively (Table 3 and Figure S3c; J_{SC}, V_{OC}, and FF plots are also shown in Figure S3d–f). Reducing the k_{BMR} further to 10^{-12} cm^3 s^{-1} (case 2), leads to a DJ cell with PCE of nearly 20%. To this end, owing to the recent development of Y6 NFA[3] and its derivatives,[10,21,22] high PCEs > 18% have been reported with very low energy loss for OPV ($E_{loss} \approx 0.5$ eV;[4,10] energy loss in OPV is typically between 0.7 and 1 eV),[67] which makes it appealing as a BC in the DJ-OPVs. For comparison, the PTB7-Th:CO$_i$8DFIC:PC$_{71}$BM blend which has a similar E_g with PM6:Y6 exhibits higher energy loss of ~0.6 V. Our simulation predicts (Table 3) that DJ devices composed of BC with similar absorption profile to Y6-based blend (**BC2**, case 3) and with low energy loss (~0.5 eV) could potentially reach higher PCEs of >21%. We also note that our previous calculations show that PCEs of >25% can also be achieved by DJ OPV cells by further optimizing the subcells' optical bandgap, increasing the charge mobilities ($\geq 10^{-3}$ cm^2 V^{-1} s^{-1}), and further lowering k_{BMR} (10^{-12} cm^3 s^{-1}).[11]

We note that neither predicted nor experimental results indicate that the TJ device can be amenable to PCEs higher than those of the DJ solar cells probably because of the large absorption overlaps between the subcells. Because of this, the J_{SC} of the TJ device (8.4 mAcm^{-2}) significantly drops compared to the respective SJ device with the lowest J_{SC} (12.5 mAcm^{-2}, Table 2). To better understand the optimal subcell bandgap combinations and the practical efficiency limits of TJ OPVs, we combined the optical transfer matrix modeling with drift-diffusion electrical modeling. As shown in Figure S4a, the absorption profiles of the BHJs used for the FC, MC, and BC were chosen to be complementary with their bandgaps ranging from 1.2 to 2 eV. Specifically, their bandgaps were set as 2 or 1.7 eV (for FC), 1.57 or 1.46 eV (for MC), and 1.3 or 1.2 eV (for BC), respectively. Similar to our previous calculation,[11] we assume that the charge-transfer energy (E_{CT}) values used to account for the V_{OC} in our simulation follow the relation $E_{CT} = E_g - 0.05$ eV (see Table 3). The results presented in Figure S4b,c and summarized in Table 3 indicate that high PCE values of up to 24% (case 2: $\mu_h = \mu_e = 5 \times 10^{-4}$ cm^2 V^{-1} s^{-1} and IQE = 90%) and up to 26% (case 10: $\mu_h = \mu_e = 10^{-3}$ cm^2 V^{-1} s^{-1} and IQE = 95%) can be achieved when FC, MC, and BC with optical bandgaps of 2, 1.57, and 1.2 eV are used (Table 3) and assuming a k_{BMR} of 10^{-12} cm^3 s^{-1}. The aforementioned PCE values were calculated assuming no losses from series and shunt resistance, which results in a high FF of up to 89%. If the effect of these parasitic resistances is considered and assuming an FF of 81% (currently achievable for OPVs[21,68]), the predicted PCE of the TJ OPV becomes 22.4% and 23.9% for cases 2 and 10, respectively.

The optimum subcell's thicknesses and simulated results for different subcell bandgap combinations are also shown in Table 3. The simulated PCE is 19.4% (J_{SC} = 8.13 mAcm^{-2}) for FC/MC/BC bandgap combination of 1.7/1.57/1.3 eV (Table 3, case 5, $\mu_h = \mu_e = 5 \times 10^{-4}$ cm^2 V^{-1} s^{-1}). The PCE increases significantly to 24.1% (J_{SC} = 9.6 mAcm^{-2}) if the FC's bandgap is increased to 2 eV while that of the BC's is reduced to 1.2 eV (case 2), further highlighting the need to reduce the absorption overlap between subcells. Importantly, we note that efficient NFA-based OPVs that combine a bandgap of >1.7 eV with electron mobility of $>10^{-4}$ cm^2 V^{-1} s^{-1} are scarce, as can clearly be seen in Figure S5 where we plot the μ_e versus the optical bandgap of NFAs-based BHJs reported to date in the literature. This is an important observation that highlights the need for developing wider bandgap organic BHJs, particularly for use in multijunction OPVs.

In summary, we have developed DJ NFA-based OPVs with a maximum PCE of 16.5% in excellent agreement with our theoretical predictions. The high efficiency along with the excellent V_{OC} (1.66 V), high J_{SC} (13.9 mAcm^{-2}), and good FF (71.8%) positions our devices among the best-performing DJ OPVs reported to date.[13,17] Going a step further, we developed TJ OPVs utilizing PBDB-T:F-M as the FC, PM6:IT-4F as the MC, and PTB7-Th:CO$_i$8DFIC:PC$_{71}$BM as the BC. Optimized cells yielded a PCE of 14.9%; a high V_{OC} of 2.49 V; a J_{SC} of 8.42 mA cm^{-2}; and a remarkable, for a TJ OPV, FF of 71%. Our device modeling suggests three design rules that can aid further development of high-performance multijunction OPV devices:

(i) Increasing the carrier mobilities of the active-layer used as FC to $\geq 5 \times 10^{-4}$ cm^2 V^{-1} s^{-1} is needed to boost the DJ and TJ OPVs performance further.

(ii) Strong absorption overlap in TJ devices remains a major issue, and minimizing the photon competition between subcells is required to increase the performance of TJ OPVs further (e.g., calculated optimal optical bandgaps are 2, 1.57, and 1.2 eV for FC, MC, and BC, respectively).

(iii) TJ OPVs have the potential to reach PCE values up to 26% by increasing the carrier mobilities to $>10^{-3}$ cm^2 V^{-1} s^{-1} while simultaneously reducing k_{BMR} to 10^{-12} cm^3 s^{-1} for all subcells. Newly developed approaches, such as molecular doping of the BHJ,[9] could help achieve this target.

The present study provides important insights into cell design aspects while highlighting practical guidelines for the development of next-generation multijunction NFA-based OPVs.

https://dx.doi.org/10.1021/acsenergylett.0c02077
ACS Energy Lett. 2020, 5, 3692–3701

■ ASSOCIATED CONTENT

Supporting Information

The Supporting Information is available free of charge at https://pubs.acs.org/doi/10.1021/acsenergylett.0c02077.

Materials, device fabrication, characterization and simulation details; optical constant and $J-V$ of single-cells used for simulation; double-junction OPV devices reported in the last five years; measured and simulated FF and J_{SC} of PBDB-T:IDTTA devices for different thicknesses; input parameters used for simulations; triple-junction simulation; and electron mobility of nonfullerene-based devices versus energy bandgap from the literature (PDF)

■ AUTHOR INFORMATION

Corresponding Authors

Yuliar Firdaus − *King Abdullah University of Science and Technology (KAUST), Physical Sciences and Engineering Division (PSE), KAUST Solar Center (KSC), Thuwal 23955-6900, Saudi Arabia*; Email: yuliar.firdaus@kaust.edu.sa

Thomas D. Anthopoulos − *King Abdullah University of Science and Technology (KAUST), Physical Sciences and Engineering Division (PSE), KAUST Solar Center (KSC), Thuwal 23955-6900, Saudi Arabia*; orcid.org/0000-0002-0978-8813; Email: thomas.anthopoulos@kaust.edu.sa

Authors

Carr Hoi Yi Ho − *Department of Materials Science and Engineering, and Organic and Carbon Electronics Laboratories (ORaCEL), North Carolina State University, Raleigh, North Carolina 27695, United States*

Yuanbao Lin − *King Abdullah University of Science and Technology (KAUST), Physical Sciences and Engineering Division (PSE), KAUST Solar Center (KSC), Thuwal 23955-6900, Saudi Arabia*

Emre Yengel − *King Abdullah University of Science and Technology (KAUST), Physical Sciences and Engineering Division (PSE), KAUST Solar Center (KSC), Thuwal 23955-6900, Saudi Arabia*; orcid.org/0000-0001-7208-4803

Vincent M. Le Corre − *Zernike Institute for Advanced Materials, University of Groningen, 9747 AG Groningen, The Netherlands*; orcid.org/0000-0001-6365-179X

Mohamad I. Nugraha − *King Abdullah University of Science and Technology (KAUST), Physical Sciences and Engineering Division (PSE), KAUST Solar Center (KSC), Thuwal 23955-6900, Saudi Arabia*; orcid.org/0000-0001-9352-1902

Emre Yarali − *King Abdullah University of Science and Technology (KAUST), Physical Sciences and Engineering Division (PSE), KAUST Solar Center (KSC), Thuwal 23955-6900, Saudi Arabia*

Franky So − *Department of Materials Science and Engineering, and Organic and Carbon Electronics Laboratories (ORaCEL), North Carolina State University, Raleigh, North Carolina 27695, United States*; orcid.org/0000-0002-8310-677X

Complete contact information is available at: https://pubs.acs.org/10.1021/acsenergylett.0c02077

Notes

The authors declare no competing financial interest.

■ ACKNOWLEDGMENTS

This publication is based upon work supported by the King Abdullah University of Science and Technology (KAUST) Office of Sponsored Research (OSR) under Award No: OSR-2018-CARF/CCF-3079; Office of Naval Research Grant N00014-17-1-2242; National Science Foundation Award CBET-1639429; and NextGen Nano Limited.

■ REFERENCES

(1) Lin, Y.; Wang, J.; Zhang, Z.-G.; Bai, H.; Li, Y.; Zhu, D.; Zhan, X. An Electron Acceptor Challenging Fullerenes for Efficient Polymer Solar Cells. *Adv. Mater.* **2015**, *27* (7), 1170−1174.

(2) Zhao, W.; Li, S.; Yao, H.; Zhang, S.; Zhang, Y.; Yang, B.; Hou, J. Molecular Optimization Enables over 13% Efficiency in Organic Solar Cells. *J. Am. Chem. Soc.* **2017**, *139* (21), 7148−7151.

(3) Yuan, J.; Zhang, Y.; Zhou, L.; Zhang, G.; Yip, H.-L.; Lau, T.-K.; Lu, X.; Zhu, C.; Peng, H.; Johnson, P. A.; Leclerc, M.; Cao, Y.; Ulanski, J.; Li, Y.; Zou, Y. Single-Junction Organic Solar Cell with over 15% Efficiency Using Fused-Ring Acceptor with Electron-Deficient Core. *Joule* **2019**, *3* (4), 1140−1151.

(4) Liu, Q.; Jiang, Y.; Jin, K.; Qin, J.; Xu, J.; Li, W.; Xiong, J.; Liu, J.; Xiao, Z.; Sun, K.; Yang, S.; Zhang, X.; Ding, L. 18% Efficiency organic solar cells. *Science Bulletin* **2020**, *65* (4), 272−275.

(5) An, Q.; Wang, J.; Gao, W.; Ma, X.; Hu, Z.; Gao, J.; Xu, C.; Hao, M.; Zhang, X.; Yang, C.; Zhang, F. Alloy-like ternary polymer solar cells with over 17.2% efficiency. *Science Bulletin* **2020**, *65* (7), 538−545.

(6) Zhan, L.; Li, S.; Lau, T.-K.; Cui, Y.; Lu, X.; Shi, M.; Li, C.-Z.; Li, H.; Hou, J.; Chen, H. Over 17% efficiency ternary organic solar cells enabled by two non-fullerene acceptors working in an alloy-like model. *Energy Environ. Sci.* **2020**, *13* (2), 635−645.

(7) Lin, Y.; Adilbekova, B.; Firdaus, Y.; Yengel, E.; Faber, H.; Sajjad, M.; Zheng, X.; Yarali, E.; Seitkhan, A.; Bakr, O. M.; El-Labban, A.; Schwingenschlögl, U.; Tung, V.; McCulloch, I.; Laquai, F.; Anthopoulos, T. D. 17% Efficient Organic Solar Cells Based on Liquid Exfoliated WS2 as a Replacement for PEDOT:PSS. *Adv. Mater.* **2019**, *31* (46), 1902965.

(8) Firdaus, Y.; Le Corre, V. M.; Karuthedath, S.; Liu, W.; Markina, A.; Huang, W.; Chattopadhyay, S.; Nahid, M. M.; Nugraha, M. I.; Lin, Y.; Seitkhan, A.; Basu, A.; Zhang, W.; McCulloch, I.; Ade, H.; Labram, J.; Laquai, F.; Andrienko, D.; Koster, L. J. A.; Anthopoulos, T. D. Long-range exciton diffusion in molecular non-fullerene acceptors. *Nat. Commun.* **2020**, *11* (1), 5220.

(9) Lin, Y.; Firdaus, Y.; Nugraha, M. I.; Liu, F.; Karuthedath, S.; Emwas, A.-H.; Zhang, W.; Seitkhan, A.; Neophytou, M.; Faber, H.; Yengel, E.; McCulloch, I.; Tsetseris, L.; Laquai, F.; Anthopoulos, T. D. 17.1% Efficient Single-Junction Organic Solar Cells Enabled by n-Type Doping of the Bulk-Heterojunction. *Adv. Sci.* **2020**, *7* (7), 1903419.

(10) Lin, Y.; Firdaus, Y.; Isikgor, F. H.; Nugraha, M. I.; Yengel, E.; Harrison, G. T.; Hallani, R.; El-Labban, A.; Faber, H.; Ma, C.; Zheng, X.; Subbiah, A.; Howells, C. T.; Bakr, O. M.; McCulloch, I.; Wolf, S. D.; Tsetseris, L.; Anthopoulos, T. D. Self-Assembled Monolayer Enables Hole Transport Layer-Free Organic Solar Cells with 18% Efficiency and Improved Operational Stability. *ACS Energy Letters* **2020**, *5* (9), 2935−2944.

(11) Firdaus, Y.; Le Corre, V. M.; Khan, J. I.; Kan, Z.; Laquai, F.; Beaujuge, P. M.; Anthopoulos, T. D. Key Parameters Requirements for Non-Fullerene-Based Organic Solar Cells with Power Conversion Efficiency > 20%. *Adv. Sci.* **2019**, *6* (9), 1802028.

(12) Firdaus, Y.; He, Q.; Lin, Y.; Nugroho, F. A. A.; Le Corre, V. M.; Yengel, E.; Balawi, A. H.; Seitkhan, A.; Laquai, F.; Langhammer, C.; Liu, F.; Heeney, M.; Anthopoulos, T. D. Novel wide-bandgap non-fullerene acceptors for efficient tandem organic solar cells. *J. Mater. Chem. A* **2020**, *8* (3), 1164−1175.

(13) Ho, C. H. Y.; Kim, T.; Xiong, Y.; Firdaus, Y.; Yi, X.; Dong, Q.; Rech, J. J.; Gadisa, A.; Booth, R.; O'Connor, B. T.; Amassian, A.; Ade, H.; You, W.; Anthopoulos, T. D.; So, F. High-Performance Tandem Organic Solar Cells Using HSolar as the Interconnecting Layer. *Adv. Energy Mater.* **2020**, *10*, 2000823.
(14) Dennler, G.; Prall, H.-J.; Koeppe, R.; Egginger, M.; Autengruber, R.; Sariciftci, N. S. Enhanced spectral coverage in tandem organic solar cells. *Appl. Phys. Lett.* **2006**, *89* (7), 073502.
(15) Kim, T.; Palmiano, E.; Liang, R.-Z.; Hu, H.; Murali, B.; Kirmani, A. R.; Firdaus, Y.; Gao, Y.; Sheikh, A.; Yuan, M.; Mohammed, O. F.; Hoogland, S.; Beaujuge, P. M.; Sargent, E. H.; Amassian, A. Hybrid tandem quantum dot/organic photovoltaic cells with complementary near infrared absorption. *Appl. Phys. Lett.* **2017**, *110* (22), 223903.
(16) Kim, T.; Firdaus, Y.; Kirmani, A. R.; Liang, R.-Z.; Hu, H.; Liu, M.; El Labban, A.; Hoogland, S.; Beaujuge, P. M.; Sargent, E. H.; Amassian, A. Hybrid Tandem Quantum Dot/Organic Solar Cells with Enhanced Photocurrent and Efficiency via Ink and Interlayer Engineering. *ACS Energy Letters* **2018**, *3* (6), 1307−1314.
(17) Meng, L.; Zhang, Y.; Wan, X.; Li, C.; Zhang, X.; Wang, Y.; Ke, X.; Xiao, Z.; Ding, L.; Xia, R.; Yip, H.-L.; Cao, Y.; Chen, Y. Organic and solution-processed tandem solar cells with 17.3% efficiency. *Science* **2018**, *361* (6407), 1094−1098.
(18) Huang, W.; Chang, S.-Y.; Cheng, P.; Meng, D.; Zhu, B.; Nuryyeva, S.; Zhu, C.; Huo, L.; Wang, Z.; Wang, M.; Yang, Y. High Efficiency Non-fullerene Organic Tandem Photovoltaics Based on Ternary Blend Subcells. *Nano Lett.* **2018**, *18* (12), 7977−7984.
(19) Chen, F.-X.; Qin, R.; Xia, R.; Zhang, Y.; Zuo, L.; Yip, H.-L.; Chen, H.; Li, C.-Z. Toward Efficient Triple-Junction Polymer Solar Cells through Rational Selection of Middle Cells. *ACS Energy Letters* **2020**, *5* (6), 1771−1779.
(20) Zhang, Y.; Kan, B.; Sun, Y.; Wang, Y.; Xia, R.; Ke, X.; Yi, Y.-Q.-Q.; Li, C.; Yip, H.-L.; Wan, X.; Cao, Y.; Chen, Y. Nonfullerene Tandem Organic Solar Cells with High Performance of 14.11%. *Adv. Mater.* **2018**, *30* (18), 1707508.
(21) Cui, Y.; Yao, H.; Zhang, J.; Xian, K.; Zhang, T.; Hong, L.; Wang, Y.; Xu, Y.; Ma, K.; An, C.; He, C.; Wei, Z.; Gao, F.; Hou, J. Single-Junction Organic Photovoltaic Cells with Approaching 18% Efficiency. *Adv. Mater.* **2020**, *32* (19), 1908205.
(22) Cui, Y.; Yao, H.; Zhang, J.; Zhang, T.; Wang, Y.; Hong, L.; Xian, K.; Xu, B.; Zhang, S.; Peng, J.; Wei, Z.; Gao, F.; Hou, J. Over 16% efficiency organic photovoltaic cells enabled by a chlorinated acceptor with increased open-circuit voltages. *Nat. Commun.* **2019**, *10* (1), 2515.
(23) Di Carlo Rasi, D.; Janssen, R. A. J. Advances in Solution-Processed Multijunction Organic Solar Cells. *Adv. Mater.* **2019**, *31* (10), 1806499.
(24) Li, H.; Xiao, Z.; Ding, L.; Wang, J. Thermostable single-junction organic solar cells with a power conversion efficiency of 14.62%. *Science Bulletin* **2018**, *63* (6), 340−342.
(25) Gao, Y.; Le Corre, V. M.; Gaïtis, A.; Neophytou, M.; Hamid, M. A.; Takanabe, K.; Beaujuge, P. M. Homo-Tandem Polymer Solar Cells with VOC > 1.8 V for Efficient PV-Driven Water Splitting. *Adv. Mater.* **2016**, *28* (17), 3366−3373.
(26) Hadipour, A.; de Boer, B.; Blom, P. W. M. Device operation of organic tandem solar cells. *Org. Electron.* **2008**, *9* (5), 617−624.
(27) Becker, T.; Trost, S.; Behrendt, A.; Shutsko, I.; Polywka, A.; Görrn, P.; Reckers, P.; Das, C.; Mayer, T.; Di Carlo Rasi, D.; Hendriks, K. H.; Wienk, M. M.; Janssen, R. A. J.; Riedl, T. All-Oxide MoOx/SnOx Charge Recombination Interconnects for Inverted Organic Tandem Solar Cells. *Adv. Energy Mater.* **2018**, *8* (10), 1702533.
(28) Che, X.; Li, Y.; Qu, Y.; Forrest, S. R. High fabrication yield organic tandem photovoltaics combining vacuum- and solution-processed subcells with 15% efficiency. *Nat. Energy* **2018**, *3* (5), 422−427.
(29) Chen, S.-C.; Zheng, Q.; Yin, Z.; Cai, D.; Ma, Y. High performance thermal-treatment-free tandem polymer solar cells with high fill factors. *Org. Electron.* **2017**, *47*, 79−84.
(30) Cheng, P.; Liu, Y.; Chang, S.-Y.; Li, T.; Sun, P.; Wang, R.; Cheng, H.-W.; Huang, T.; Meng, L.; Nuryyeva, S.; Zhu, C.; Wei, K.-H.; Sun, B.; Zhan, X.; Yang, Y. Efficient Tandem Organic Photovoltaics with Tunable Rear Sub-cells. *Joule* **2019**, *3* (2), 432−442.
(31) Cui, Y.; Xu, B.; Yang, B.; Yao, H.; Li, S.; Hou, J. A Novel pH Neutral Self-Doped Polymer for Anode Interfacial Layer in Efficient Polymer Solar Cells. *Macromolecules* **2016**, *49* (21), 8126−8133.
(32) Cui, Y.; Yao, H.; Gao, B.; Qin, Y.; Zhang, S.; Yang, B.; He, C.; Xu, B.; Hou, J. Fine-Tuned Photoactive and Interconnection Layers for Achieving over 13% Efficiency in a Fullerene-Free Tandem Organic Solar Cell. *J. Am. Chem. Soc.* **2017**, *139* (21), 7302−7309.
(33) Gao, Y.; Jin, F.; Li, W.; Su, Z.; Chu, B.; Wang, J.; Zhao, H.; Wu, H.; Liu, C.; Hou, F.; Lin, T.; Song, Q. Highly efficient organic tandem solar cell with a SubPc interlayer based on TAPC:C70 bulk heterojunction. *Sci. Rep.* **2016**, *6* (1), 23916.
(34) Guo, B.; Guo, X.; Li, W.; Meng, X.; Ma, W.; Zhang, M.; Li, Y. A wide-bandgap conjugated polymer for highly efficient inverted single and tandem polymer solar cells. *J. Mater. Chem. A* **2016**, *4* (34), 13251−13258.
(35) Guo, B.; Li, W.; Luo, G.; Guo, X.; Yao, H.; Zhang, M.; Hou, J.; Li, Y.; Wong, W.-Y. Exceeding 14% Efficiency for Solution-Processed Tandem Organic Solar Cells Combining Fullerene- and Nonfullerene-Based Subcells with Complementary Absorption. *ACS Energy Letters* **2018**, *3* (10), 2566−2572.
(36) Huang, X.; Sun, B.; Li, Y.; Jiang, C.; Fan, D.; Fan, J.; Forrest, S. R. 15.9% organic tandem solar cell with extended near-infrared absorption. *Appl. Phys. Lett.* **2020**, *116* (15), 153501.
(37) Kang, R.; Park, S.; Jung, Y. K.; Lim, D. C.; Cha, M. J.; Seo, J. H.; Cho, S. High-Efficiency Polymer Homo-Tandem Solar Cells with Carbon Quantum-Dot-Doped Tunnel Junction Intermediate Layer. *Adv. Energy Mater.* **2018**, *8* (10), 1702165.
(38) Lee, J.; Kang, H.; Kee, S.; Lee, S. H.; Jeong, S. Y.; Kim, G.; Kim, J.; Hong, S.; Back, H.; Lee, K. Long-Term Stable Recombination Layer for Tandem Polymer Solar Cells Using Self-Doped Conducting Polymers. *ACS Appl. Mater. Interfaces* **2016**, *8* (9), 6144−6151.
(39) Li, M.; Gao, K.; Wan, X.; Zhang, Q.; Kan, B.; Xia, R.; Liu, F.; Yang, X.; Feng, H.; Ni, W.; Wang, Y.; Peng, J.; Zhang, H.; Liang, Z.; Yip, H.-L.; Peng, X.; Cao, Y.; Chen, Y. Solution-processed organic tandem solar cells with power conversion efficiencies > 12%. *Nat. Photonics* **2017**, *11* (2), 85−90.
(40) Li, T.-y.; Meyer, T.; Ma, Z.; Benduhn, J.; Körner, C.; Zeika, O.; Vandewal, K.; Leo, K. Small Molecule Near-Infrared Boron Dipyrromethene Donors for Organic Tandem Solar Cells. *J. Am. Chem. Soc.* **2017**, *139* (39), 13636−13639.
(41) Li, Y.; Lin, J.-D.; Liu, X.; Qu, Y.; Wu, F.-P.; Liu, F.; Jiang, Z.-Q.; Forrest, S. R. Near-Infrared Ternary Tandem Solar Cells. *Adv. Mater.* **2018**, *30* (45), 1804416.
(42) Liu, G.; Jia, J.; Zhang, K.; Jia, X. e.; Yin, Q.; Zhong, W.; Li, L.; Huang, F.; Cao, Y. 15% Efficiency Tandem Organic Solar Cell Based on a Novel Highly Efficient Wide-Bandgap Nonfullerene Acceptor with Low Energy Loss. *Adv. Energy Mater.* **2019**, *9* (11), 1803657.
(43) Liu, W.; Li, S.; Huang, J.; Yang, S.; Chen, J.; Zuo, L.; Shi, M.; Zhan, X.; Li, C.-Z.; Chen, H. Nonfullerene Tandem Organic Solar Cells with High Open-Circuit Voltage of 1.97 V. *Adv. Mater.* **2016**, *28* (44), 9729−9734.
(44) Qin, Y.; Chen, Y.; Cui, Y.; Zhang, S.; Yao, H.; Huang, J.; Li, W.; Zheng, Z.; Hou, J. Achieving 12.8% Efficiency by Simultaneously Improving Open-Circuit Voltage and Short-Circuit Current Density in Tandem Organic Solar Cells. *Adv. Mater.* **2017**, *29* (24), 1606340.
(45) Shi, Z.; Liu, H.; Li, J.; Wang, F.; Bai, Y.; Bian, X.; Zhang, B.; Alsaedi, A.; Hayat, T.; Tan, Z. a. Engineering the interconnecting layer for efficient inverted tandem polymer solar cells with absorption complementary fullerene and nonfullerene acceptors. *Sol. Energy Mater. Sol. Cells* **2018**, *180*, 1−9.
(46) Yao, H.; Chen, Y.; Qin, Y.; Yu, R.; Cui, Y.; Yang, B.; Li, S.; Zhang, K.; Hou, J. Design and Synthesis of a Low Bandgap Small Molecule Acceptor for Efficient Polymer Solar Cells. *Adv. Mater.* **2016**, *28* (37), 8283−8287.

https://dx.doi.org/10.1021/acsenergylett.0c02077
ACS Energy Lett. 2020, 5, 3692−3701

(47) Yuan, J.; Ford, M. J.; Xu, Y.; Zhang, Y.; Bazan, G. C.; Ma, W. Improved Tandem All-Polymer Solar Cells Performance by Using Spectrally Matched Subcells. *Adv. Energy Mater.* **2018**, *8* (14), 1703291.
(48) Yuan, J.; Gu, J.; Shi, G.; Sun, J.; Wang, H.-Q.; Ma, W. High efficiency all-polymer tandem solar cells. *Sci. Rep.* **2016**, *6* (1), 26459.
(49) Yue, Q.; Zhou, Z.; Xu, S.; Zhang, J.; Zhu, X. Design and synthesis of medium-bandgap small-molecule electron acceptors for efficient tandem solar cells. *J. Mater. Chem. A* **2018**, *6* (28), 13588−13592.
(50) Zhang, K.; Fan, B.; Xia, R.; Liu, X.; Hu, Z.; Gu, H.; Liu, S.; Yip, H.-L.; Ying, L.; Huang, F.; Cao, Y. Highly Efficient Tandem Organic Solar Cell Enabled by Environmentally Friendly Solvent Processed Polymeric Interconnecting Layer. *Adv. Energy Mater.* **2018**, *8* (15), 1703180.
(51) Zhang, K.; Gao, K.; Xia, R.; Wu, Z.; Sun, C.; Cao, J.; Qian, L.; Li, W.; Liu, S.; Huang, F.; Peng, X.; Ding, L.; Yip, H.-L.; Cao, Y. High-Performance Polymer Tandem Solar Cells Employing a New n-Type Conjugated Polymer as an Interconnecting Layer. *Adv. Mater.* **2016**, *28* (24), 4817−4823.
(52) Zhang, K.; Xia, R.; Fan, B.; Liu, X.; Wang, Z.; Dong, S.; Yip, H.-L.; Ying, L.; Huang, F.; Cao, Y. 11.2% All-Polymer Tandem Solar Cells with Simultaneously Improved Efficiency and Stability. *Adv. Mater.* **2018**, *30* (36), 1803166.
(53) Zhang, Q.; Wan, X.; Liu, F.; Kan, B.; Li, M.; Feng, H.; Zhang, H.; Russell, T. P.; Chen, Y. Evaluation of Small Molecules as Front Cell Donor Materials for High-Efficiency Tandem Solar Cells. *Adv. Mater.* **2016**, *28* (32), 7008−7012.
(54) Zhang, S.; Qin, Y.; Uddin, M. A.; Jang, B.; Zhao, W.; Liu, D.; Woo, H. Y.; Hou, J. A Fluorinated Polythiophene Derivative with Stabilized Backbone Conformation for Highly Efficient Fullerene and Non-Fullerene Polymer Solar Cells. *Macromolecules* **2016**, *49* (8), 2993−3000.
(55) Zheng, Z.; Zhang, S.; Zhang, J.; Qin, Y.; Li, W.; Yu, R.; Wei, Z.; Hou, J. Over 11% Efficiency in Tandem Polymer Solar Cells Featured by a Low-Band-Gap Polymer with Fine-Tuned Properties. *Adv. Mater.* **2016**, *28* (25), 5133−5138.
(56) Che, X.; Xiao, X.; Zimmerman, J. D.; Fan, D.; Forrest, S. R. High-Efficiency, Vacuum-Deposited, Small-Molecule Organic Tandem and Triple-Junction Photovoltaic Cells. *Adv. Energy Mater.* **2014**, *4* (18), 1400568.
(57) Chen, C.-C.; Chang, W.-H.; Yoshimura, K.; Ohya, K.; You, J.; Gao, J.; Hong, Z.; Yang, Y. An Efficient Triple-Junction Polymer Solar Cell Having a Power Conversion Efficiency Exceeding 11%. *Adv. Mater.* **2014**, *26* (32), 5670−5677.
(58) Di Carlo Rasi, D.; Hendriks, K. H.; Wienk, M. M.; Janssen, R. A. J. Accurate Characterization of Triple-Junction Polymer Solar Cells. *Adv. Energy Mater.* **2017**, *7* (22), 1701664.
(59) Li, W.; Furlan, A.; Hendriks, K. H.; Wienk, M. M.; Janssen, R. A. J. Efficient Tandem and Triple-Junction Polymer Solar Cells. *J. Am. Chem. Soc.* **2013**, *135* (15), 5529−5532.
(60) Meerheim, R.; Körner, C.; Oesen, B.; Leo, K. 10.4% Efficient triple organic solar cells containing near infrared absorbers. *Appl. Phys. Lett.* **2016**, *108* (10), 103302.
(61) Yusoff, A. R. b. M.; Kim, D.; Kim, H. P.; Shneider, F. K.; da Silva, W. J.; Jang, J. A high efficiency solution processed polymer inverted triple-junction solar cell exhibiting a power conversion efficiency of 11.83%. *Energy Environ. Sci.* **2015**, *8* (1), 303−316.
(62) Esiner, S.; van Eersel, H.; Wienk, M. M.; Janssen, R. A. J. Triple Junction Polymer Solar Cells for Photoelectrochemical Water Splitting. *Adv. Mater.* **2013**, *25* (21), 2932−2936.
(63) Zhang, S.; Qin, Y.; Zhu, J.; Hou, J. Over 14% Efficiency in Polymer Solar Cells Enabled by a Chlorinated Polymer Donor. *Adv. Mater.* **2018**, *30* (20), 1800868.
(64) Khan, J. I.; Firdaus, Y.; Cruciani, F.; Liu, S.; Anthopoulos, T. D.; Beaujuge, P. M.; Laquai, F. Thienyl Sidechain Substitution and Backbone Fluorination of Benzodithiophene-Based Donor Polymers Concertedly Minimize Carrier Losses in ITIC-Based Organic Solar Cells. *J. Phys. Chem. C* **2020**, *124* (19), 10420−10429.
(65) Karuthedath, S.; Firdaus, Y.; Liang, R.-Z.; Gorenflot, J.; Beaujuge, P. M.; Anthopoulos, T. D.; Laquai, F. Impact of Fullerene on the Photophysics of Ternary Small Molecule Organic Solar Cells. *Adv. Energy Mater.* **2019**, *9* (33), 1901443.
(66) Wetzelaer, G.-J. A. H.; Van der Kaap, N. J.; Koster, L. J. A.; Blom, P. W. M. Quantifying Bimolecular Recombination in Organic Solar Cells in Steady State. *Adv. Energy Mater.* **2013**, *3* (9), 1130−1134.
(67) He, B.; Yang, B.; Kolaczkowski, M. A.; Anderson, C. A.; Klivansky, L. M.; Chen, T. L.; Brady, M. A.; Liu, Y. Molecular Engineering for Large Open-Circuit Voltage and Low Energy Loss in Around 10% Non-fullerene Organic Photovoltaics. *ACS Energy Letters* **2018**, *3* (4), 1028−1035.
(68) Zheng, Z.; Hu, Q.; Zhang, S.; Zhang, D.; Wang, J.; Xie, S.; Wang, R.; Qin, Y.; Li, W.; Hong, L.; Liang, N.; Liu, F.; Zhang, Y.; Wei, Z.; Tang, Z.; Russell, T. P.; Hou, J.; Zhou, H. A Highly Efficient Non-Fullerene Organic Solar Cell with a Fill Factor over 0.80 Enabled by a Fine-Tuned Hole-Transporting Layer. *Adv. Mater.* **2018**, *30* (34), 1801801.

https://dx.doi.org/10.1021/acsenergylett.0c02077
ACS Energy Lett. 2020, 5, 3692−3701